Research article
UDC 612.843.31
https://doi.org/10.21702/rpj.2024.1.1

Colour discrimination in post-COVID-19 observers assessed by the Farnsworth-Munsell 100-Hue test

Yulia A. Griber[1*], Galina V. Paramei[2]

[1] Smolensk State University, Smolensk, Russian Federation
[2] Liverpool Hope University, Liverpool, United Kingdom

[*]Corresponding author: y.griber@gmail.com

Abstract

Introduction. Post-COVID-19, various ophthalmological symptoms and visual impairments have been reported. We hypothesised that colour vision may be affected too. **Methods.** We assessed colour discrimination using the Farnsworth-Munsell 100 Hue test (FM-100) in individuals who have had COVID-19 (N = 77; 18–68 years). **Results.** Total error score (TES) indicated superior colour discrimination in 34 observers. The Vingrys–King-Smith C-index (severity) exceeded the normal cut-off measure in 44 observers. In participants (N = 35) with average TES, the Vingrys–King-Smith analysis revealed subtle colour deficiencies – either a mild tritan defect ('blue' or blue-yellow) or moderate defect with a diffuse error pattern. A minor sub-sample manifested poor discrimination (N = 6) or colour vision loss (N = 2), with a tritan or diffuse error pattern. √TES negatively correlated with the post-illness period. In partial error score (√PES), B–Y errors prevailed, regardless of the elapsed post-illness period. **Discussion.** Overall, the results indicate that about half of those who have recovered from COVID-19 revealed mild Type III acquired colour discrimination loss, characteristic of retinal disorders and vascular disease. Conceivably, coronavirus infection caused hypoperfusion (reduced vascular supply) at the retinal and/or post-retinal stages of the visual system and affected neural mechanisms of colour discrimination. The mild impairment appears to be reversible with a favourite prognosis.

Keywords

colour vision, colour perception, chromatic discrimination, COVID-19, post-COVID syndrome, Farnsworth-Munsell 100-Hue test, Type III acquired colour vision deficiency

Funding

The research was supported by Russian Science Foundation (project No. 22-18-00407, https://rscf.ru/en/project/22-18-00407/)

For citation

Griber, Y. A., Paramei, G. V. (2024). Colour discrimination in post-COVID-19 observers assessed by the Farnsworth-Munsell 100-Hue test. *Russian Psychological Journal, 21*(1), 6-32. https://doi.org/10.21702/rpj.2024.1.1

Introduction

There is increasing evidence that patients who have recovered from COVID-19 exhibit various symptoms of visual impairment, such as photophobia, blurry vision, floaters or decreased visual acuity or tunnel vision (e.g. Gangaputra & Patel, 2020; Eleiwa et al., 2021). Clinically these symptoms were associated with various neuro-ophthalmological manifestations: raised intraocular pressure (IOP) and dilated retinal veins, the sign of retinopathy (e.g. Invernizzi et al., 2020; Costa et al., 2021). In some cases, acute macular neuroretinopathy was diagnosed (Eleiwa et al., 2021), that revealed reduced blood flow in the retina (Nagy, 2020), ischaemic optic neuropathy (Yüksel et al., 2022); also, as a vaccine reaction, optic neuritis developed, attributed to vasospasm (Haseeb et al., 2022).

In the great majority of COVID-19 related ophthalmological studies colour vision (CV) was reported to be normal. However, in a few case studies dyschromatopsia was reported, where macular neuroretinopathy was diagnosed or optic nerve involvement suggested (e.g. Clarke et al., 2021; Giacuzzo et al., 2022; Nagaratnam et al., 2022). In all cases CV loss was assessed by correct readings of the Ishihara plates (e.g. 10/17). Notably, later dyschromatopsia reversed in cases of macular retinopathy (Giacuzzo et al., 2022) or unilateral optic neuritis (Richardson-May et al., 2022); however, CV worsening was recorded in a case of progressing bilateral optic neuritis (Nagaratnam et al., 2022).

To our knowledge, no systematic studies of colour sensitivity post-COVID-19 have been undertaken. In this context we venture to relate the post-COVID adverse ocular events to earlier, non-COVID, studies, which reported IOP, neuroretinopathy and optic neuritis to be accompanied by an impaired CV – either blue-yellow or non-selective discrimination loss (both blue-yellow and red-green) (e.g. Schneck & Haegerstrom-Portnoy, 1997; Castelo-Branco et al., 2004; Bimler et al., 2014). The reader is reminded of Köllner's rule (Köllner, 1912), according to which acquired blue-yellow abnormalities are likely to arise due to changes in external retinal layers, while complex dyschromatic configurations that also involve red-green loss are manifestations of conditions affecting the optic nerve (for reviews, see Verriest, 1963; Hart, 1987; Simunovic, 2016).

During the pandemic, in an online experiment we explored colour naming in post-COVID participants (pCPs), as a proxy of (affected) CV, and compared their responses with those obtained before the pandemic in healthy controls with normal CV (Griber & Paramei, 2022a; 2022b). Our study demonstrated that, compared to the controls, pCPs more frequently used names 'brown', 'green', and 'grey', as well as achromatic modifiers 'dark', 'dirty', 'pale', 'dull', and 'pastel', hinting to general "darkening" and "desaturation" of perceived colours.

The purpose of the present study was to investigate colour discrimination of pCPs using the Farnsworth-Munsell 100-Hue test (FM-100) (Farnsworth, 1943; 1957) that has been widely employed to assess CV (for reviews see Lakowski, 1969; Birch, 2001; Dain, 2004; Paramei & Bimler, 2019). The FM-100 analysis of the cap arrangement allows to quantify an observer's colour discrimination in relation to normative scores for healthy normal trichromats of the corresponding age group (Verriest et al., 1982; Knoblauch et al., 1987; Roy et al., 1991; Kinnear & Sahraie, 2002), as well as to determine the predominant axis of colour confusion (Smith et al., 1985).

In clinical practice, the FM-100 was administered to diagnose the type and severity of acquired CV deficiencies (for pioneer studies, see François & Verriest, 1961; Verriest, 1963; Birch et al., 1979). In particular, the FM-100 was employed for assessing CV impairment caused by various visual system pathologies, such as maculopathy, multiple sclerosis and optic neuritis (e.g. Vingrys & King-Smith, 1988; Ménage et al., 1993; Schneck & Haegerstrom-Portnoy, 1997; Gundogan et al., 2013), pre- and post-surgery cataract (Ao et al., 2019), and systemic diseases, such as diabetic retinopathy (Barton et al., 2004; Shoji et al., 2011; Raman et al., 2018) or hypothyroidism (Racheva et al., 2020; 2023).

Methods

Participants

Participants were volunteers – staff and students from Smolensk State University and, also, from general public recruited by advertising the study on social media. CV was assessed in 80 participants, 28 men and 52 women, who received outpatient care after having developed mild symptoms (fever and/or cough) and who had tested positive for COVID-19, certified by a doctor. Two participants had suffered from COVID-19 twice, with the confirmed diagnosis. Data of one participant with self-reported diabetes and two with congenital CV deficiency were excluded. The final data set comprised 77 observers (50 women), aged 33.58 (SD = 13.31) years (age range 18–68 years). The duration of the illness varied between 2–74 days (mean 17.82 ± 11.56 days). By the time of the FM-100 testing (March–July 2022), the elapsed period since the recovery ranged between 21–871 days, i.e. from a few weeks to 2.5 years, with mean 331 ± 217 days.

Detailed information on demographic characteristics of pCPs, as well as on their self-reports on the disease duration, changes in various sensory modalities, and the post-

COVID period are presented in Table S1 of Supplementary Materials. Almost two thirds of the participants (N = 47) reported distorted sense of smell and more than half (N = 40) a changed sense of taste during or after the illness. Some participants commented that they had experienced various symptoms of visual impairment, such as photophobia, blurry vision, decreased visual acuity or increasing astigmatism.

The study was approved by the Ethics Committee of Smolensk State University and performed in accordance with the tenets of the Declaration of Helsinki. Prior to the FM-100 testing, informed consent was obtained from all participants.

Stimuli

The FM-100 test has 85 hues, representing the full colour circle, with the hues separated by approximately equal perceptual steps. In the Munsell notation, colour caps have equal Value 6 and Chroma 6, and vary only in hue. The FM-100 (X-Rite, 2024a; 2024b; Grand Rapids, Michigan, USA) has four sets (boxes) of colour caps. There are 22 caps in box A (caps 85–21), corresponding to the hues varying from red to red-orange, and 21 colour caps in the other three boxes representing the other three sectors of colour circle: yellow to yellow-green (box B, caps 22–42), green to green-blue (box C, caps 43–63), and indigo to indigo-magenta (box D, caps 64–84). Each set contains two "anchor" colour caps, whereas the remaining caps are movable. The colour difference (ΔE) between the caps is very small, which ensures that minute differences in colour discrimination can be captured. Note though, that ΔE is not uniform between the boxes, with the box A being the least difficult and the box C the most difficult (Lakowski, 1966). The spacing of the caps is smaller around caps 85 to 8 and 35 to 65 than in the other FM-100 areas, implying a more difficult task for an observer (Dain et al., 1991).

Procedure

The procedure and data processing were implemented according to Farnsworth's original instructions (Farnsworth, 1957). The FM-100 four boxes of colour caps were presented to each individual in random order. The participant's task was to arrange the caps in a continuous colour series within each box starting from the anchor cap. Prior to the testing, the colour caps in each box were re-shuffled. The FM-100 was administered binocularly, in a laboratory close to a window, under natural daylight, which in spring–summer months in Smolensk (55°N, 32°E) provided an illuminance of ca. 1000 lux, i.e. comparable to the illumination of 1000 lux (Roy et al., 1991; Mäntyjärvi, 2001; Woo & Lee, 2002) and higher than the illumination, 200 lux, in the classical Verriest et al. study (1982). The viewing distance was 45–50 cm; near vision glasses were used if needed. All participants performed the FM-100 as novices. There was no time limit imposed; the testing session usually took 15–20 minutes.

Analysis

Colour vision was assessed by the participant's score derived from the arrangement of the caps. We calculated the following (for details see below):

1. the total error score (TES) and its square root (√TES), for the whole sample and stratified for age groups
2. partial error scores (i) for ten specified hue bands; (ii) along the B-Y and R-G axes; (iii) for different hemispheres of the FM-100 diagram
3. the moment of inertia for colour difference vectors
4. clusters of cases based on similarity of the arrangement patterns.

The total error score

The total error score (TES), which represents chromatic discrimination in general, was calculated as the sum of scores for the caps in the four boxes (Equation 1). The score for an individual cap was calculated as the sum of the absolute difference between the error number for that colour cap and the error numbers of the adjacent caps minus 2 (Farnsworth, 1957):

$$TotalErrorScore(TES) = \sum_{i=1}^{4} iES = \sum_{i=1}^{4}\left(\left(\sum_{j=1}^{n+2} CE_j\right) - \left((n+2)\cdot 2\right)\right) \quad (1)$$

where $CE_j = |C_j - C_{j-1}| + |C_j - C_{j+1}|$; i is a counter for the four boxes (i = 1 is "A", 2 is "B", 3 is "C", and 4 is "D"); C_j is the cap number of the j^{th} cap; CE_j is the cap error of the j^{th} cap; n is the number of moveable caps in the box corresponding to i (n = 22 for box A, and n = 21 for boxes B–D). For this equation to work properly, the terms $|C_j - C_{j+1}|$ and $|C_j - C_{j-1}|$ must each be equal to 1 when the caps are ordered correctly. Since the first free cap in tray A is numbered 85, not 1, the calculation requires a dummy array that assigns cap 85 a value of 1, cap 1 a value of 2, and so on. The cap error (*CE*) was calculated for the end caps of the tray, otherwise scoring would be incorrect when errors are made near the tray's ends; this necessitates the (n + 2) term in Equation (1), whereby "2" accounts for each end cap (Esposito, 2019).

Following Esposito (2019), we denoted the standard error scores for individual boxes as *AES, BES, CES* and *DES*. Thus, for an observer who placed all caps in the correct order, TES = 0; the higher the number of cap transpositions the greater is TES. Since TES has a skewed distribution, a square root transformation has been suggested to provide a distribution closer to normal (Kinnear, 1970). Hence, square root of the total error score (√TES) was used for the following analysis.

Partial error scores for specified hue bands

Guided by Ao et al. (2019), we calculated partial error scores (PES) and the corresponding √PES for the following ten hue bands (cf. Figure 3):

(1) red to yellow-red (R-YR), caps 1–9; from the long-wavelength end to 590 nm

(2) yellow-red to yellow (YR-Y), caps 10–17; 590–580 nm

(3) yellow to green-yellow (Y-GY), caps 18–26; 580–560 nm

(4) green-yellow to green (GY-G), caps 27–35; 560–500 nm

(5) green to blue-green (G-BG), caps 36–45; 500–490 nm

(6) blue-green to blue (BG-B), caps 46–53; 490–470 nm

(7) blue to purple-blue (B-PB), caps 54–60; 470 –450 nm

(8) purple-blue to purple (PB-P), caps 61–70; 450 nm to the short-wavelength end

(9) purple to red-purple (P-RP), caps 71–77; 560*–500* nm

(10) red-purple to red (RP-R), caps 78–85 (complementary to green–yellowish-green).

Partial error scores for the B-Y and R-G axes

In order to evaluate whether errors are more common along the cardinal axes of perceptual colour space, we partitioned the TES into scores along the B-Y and R-G axes (Smith et al. 1985; Knoblauch, 1987; Racheva et al., 2020; 2023). B-Y PES (caps 1–12, 34–54 and 76–85) and R-G PES (caps 13–33 and 55–75) were calculated and analysed according to Smith et al. (1985). For further analysis, the corresponding √B-Y PES and √R-G PES were used.

Partial error scores for different hemispheres of the FM-100 diagram

Since errors may concentrate along specific colour confusion axes, we also quantified the type of error by assessing error distribution in the right and left, as well as the lower and upper hemispheres of the FM-100 diagram (Farnsworth, 1957; Birch, 2001) (see Figure S2). Following the approach of Bento-Torres and colleagues (2016), the left central point corresponded to the hue axis between caps 1–43 and the right central point to the hue axis between caps 44–85, in such a way that the cumulative score in the clockwise direction in the FM-100 diagram was equal to the error median in the respective hemisphere. The

upper central point corresponded to the hue axis between caps 27–70 and the lower central point to the hue axis between caps 71–26. √PES for the corresponding FM-100 hemispheres were used for statistical analysis.

Moment of inertia

Following Vingrys & King-Smith's (1988) analysis of colour difference vectors, we calculated the moment of inertia. The analysis yields three indices, which quantify an individual cap arrangement pattern: (1) *Angle of confusion,* or orientation of the resulting radius of gyration, which identifies the type of colour deficiency; (2) *Confusion index* (*C-index*), which quantifies the severity of CV loss; and (3) *Selectivity index* (*S-index*), the ratio of the major to minor radii, which quantifies the amount of polarity or lack of randomness in a cap arrangement. For the present analysis, V&K-S's computer program, originally developed in Basic (Vingrys & King-Smith's, 1988, pp. 61–62), was re-written in Excel VBA (see Appendix 2).

Cluster analysis of post-COVID participants' FM-100 data

To explore subsamples of pCPs based on similarities of their FM-100 performance, we applied Ward's (1963) hierarchical clustering method, implemented as a program developed in scikit-learn in Python (https://scikit-learn.org/). Distances between clusters were calculated using the Ward's minimum variance criterion. We input total error scores (TES) and the three parameters of the V&K-S moment of inertia (Vingrys & King-Smith's, 1988). Our particular interest was in possible impact of the Angle on clustering outcome, since it indicates the type of CV loss and, unlike the C-index and S-index, does not correlate with TES (Bassi et al., 1993). For visualizing similarities between individual cases, t-SNE embedding initialization was applied to project high-dimensional data into a 2D map, which approximately preserves inter-item proximity, with each datapoint representing an individual participant.

Results

Total error score for post-COVID participants

Individual pCPs' total error scores (TES) are presented in Table S2 of Supplementary Materials and FM-100 diagrams in Appendix 1. Across the pCP sample, we estimated mean error scores for each cap, as illustrated in Figure 1a; since error score values are low, a magnified version of the FM-100 diagram is presented in Figure 1b. It is apparent that colour confusions prevail in the green-blue gamut (caps 40–60).

Figure 1
The FM-100 diagram for the post-COVID participants

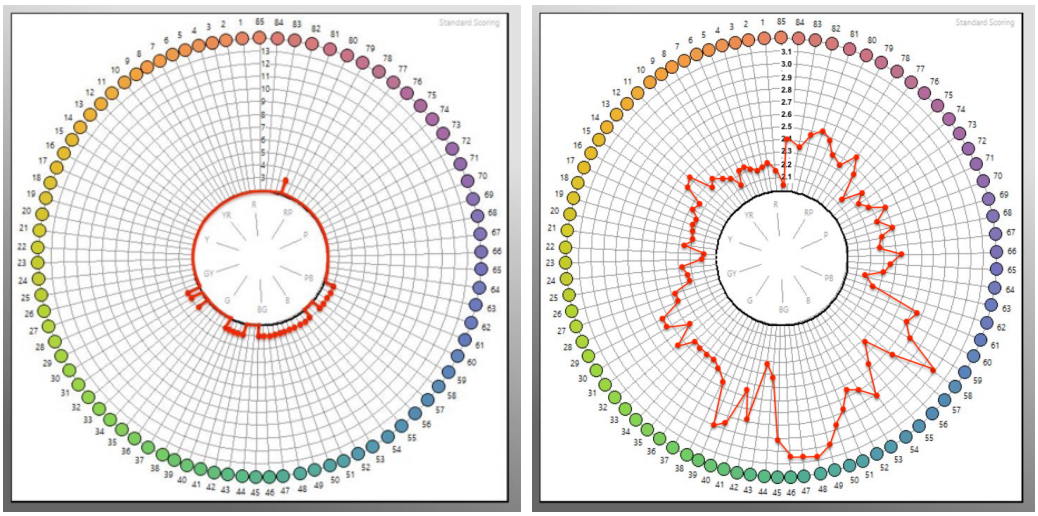

(a) (b)

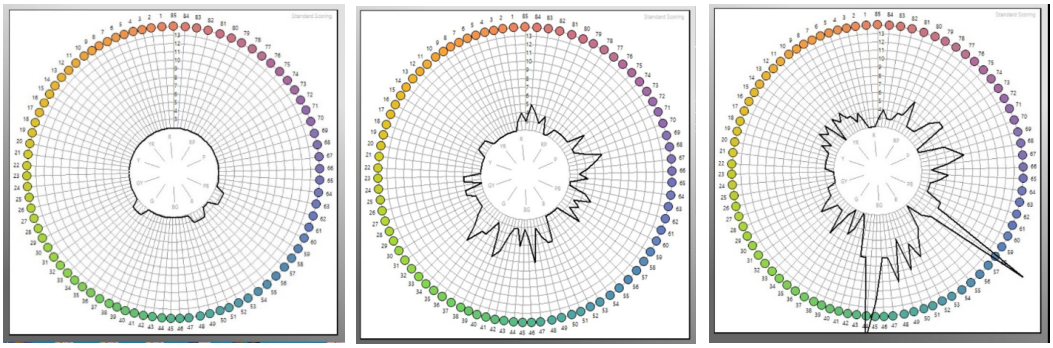

(c) (d) (e)

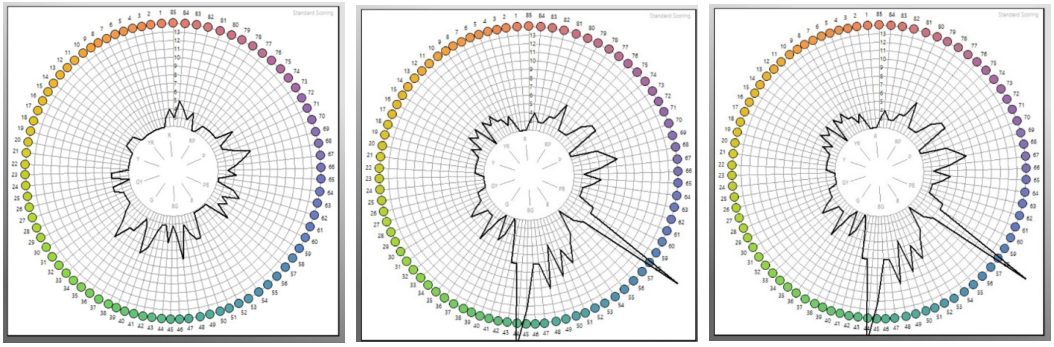

(f) (g) (h)

Note. *(a) Mean error score for each cap. (b) A magnified version of the the FM-100 diagram; note the radius scale 0–3.1 (unlike the conventional 0–13 radius scale). Exemplary FM-100 diagrams for post-COVID participants representing TES in different ranges: (c) #12: TES = 12; (d) #1: TES = 40; (e) #52: TES = 72, (f) #53: TES = 116; (g) #59: TES = 176; (h) #71: TES = 212.*

For the pCP sample, mean TES is 38.1 ± 37.8; median (mdn) is 28. However, as illustrated in Figure 1(c-h), there is a great individual variation of TES, between 0–212. Guided by Lakowski (1969), we estimated participant subsamples in relation to TES median. For more than half pCPs (N = 40), TES was ≤ 28, with superior colour discrimination (TES = 0–12) among these for 25% (N = 23). Further pCPs (N = 32; 90th percentile) demonstrated average performance, 28<TES≤ 84. Finally, TES of 5 participants (#53, 55, 59, 70, 71) was higher than the 95th percentile for their age group (Verriest, 1963); it overlaps with the subsample of 4 participants (#7, 53, 59, 71), whose TES, 116–212, >100, indicates colour deficiency (Farnsworth, 1957; Birch, 2001).

√TES mean for pCPs was 5.52 ± 2.77. Table 1 presents FM-100 means (SDs) of √TES for age-stratified groups and, for comparison, mean √TES for normal trichromats (Verriest et al., 1982; Roy et al., 1991; Kinnear & Sahraie, 2002). Table 1 indicates generally a good correspondence between the present and three earlier data sets for all age groups. Figure S1 shows √TES for individual pCPs as a function of age in relation to age groups means in (Verriest et al., 1982; Roy et al., 1991; Kinnear & Sahraie, 2002). It is noteworthy that in the 20–29 group more than half of the pCPs (16 out of 28) revealed higher mean √TES (7.98 ± 2.01) than the conservative mean √TES for the 20–29 y.o. (Verriest et al., 1982) (t = 4.56, p<0.01). Similarly, in the 30–39 pCP group almost half (5 out of 12) had higher mean √TES (8.48 ± 1.48) than the 30–39 y.o. (Verriest et al., 1982) (t = 2.69, p = 0.05).

Table 1

Mean and standard deviation of square root of the total error scores

Age group (years old)	Post-COVID participants (present study)			Healthy normal trichromats								
				Verriest et al. (1982)			Roy et al. (1991)				Kinnear & Sahraie (2002)	
	No. of observers	Mean age	Mean √TES ± SD	No. of observers	Mean age	Mean √TES ± SD	No. of observers	Right eye mean √TES ± SD	No. of observers	Left eye mean √TES ± SD	No. of observers	Mean √TES* ± SD
15–19	9	18.2	3.45 ± 1.27	32	17.3	6.63 ± 1.91	13	7.2 ± 3.0	13	6.3 ± 2.9	68	7.2 ± 2.63
20–29	28	23.1	6.02 ± 2.90	29	24.8	5.69 ± 2.07	25	6.0 ± 2.2	25	6.0 ± 2.5	35	6.7 ± 2.88
30–39	12	34.2	5.79 ± 2.92	29	34.2	6.71 ± 2.90	16	6.7 ± 1.9	17	5.8 ± 2.7	10	7.3 ± 2.38
40–49	18	44.2	5.33 ± 3.03	30	45.3	8.23 ± 2.44	13	5.8 ± 1.1	12	5.3 ± 2.0	10	8.1 ± 2.66
50–59	6	52.2	5.25 ± 2.12	30	54.2	8.68 ± 2.64	10	8.2 ± 2.0	10	8.0 ± 2.7	10	9.5 ± 2.66
60–69	4	64.3	7.17 ± 2.21	28	64.9	9.57 ± 2.44	20	10.1 ± 3.0	18	9.6 ± 3.0	10	10.7 ± 2.52

Note. *(√TES) for the post-COVID participants stratified by age groups. For comparison, also shown are √TES for age-matched healthy normal trichromats reported in (Verriest et al., 1982, Table 1), (Roy et al., 1991, Table 1), and (Kinnear & Sahraie, 2002, Table 1). We calculated mean √TES for the two youngest groups (15–19 y.o. and 20–22 y.o.) in (Kinnear & Sahraie, 2002). For all age groups, we calculated SDs based on the (weighted) age group means and 95th percentiles provided in (Kinnear & Sahraie, 2002).*

Further, across the whole pCP sample we assessed √TES as a function of the time after the recovery (Figure 2). We found a weak negative correlation, r = –0.2661, p = 0.0194, indicating an improvement of colour discrimination with increasing of the elapsed post-illness time.

Figure 2

√TES for individual post-COVID participants as a function of the time (days) elapsed after the recovery, with a line of best fit (red) and 95%-confidence interval (shaded in pink)

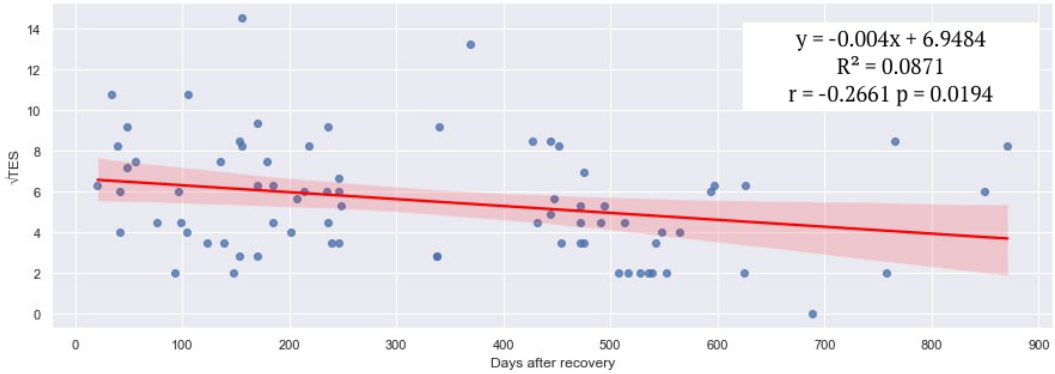

Colour discrimination in specified hue bands

For pCPs, √PES was higher in three (out of 10) of the specified hue bands, G–BG, BG–B, and B–PB, which comprise blue colours with admixtures of either green or purple (caps 36–60) (Figure 3). Note though that these bands greatly overlap with the FM-100 portion (caps 35–65), where the cap spacing is, in general, smaller (Verriest, 1963; Dain et al., 1991) and are part of box C (caps 43–63) with the lowest mean inter-cap difference (Lakowski, 1966).

To disentangle the two factors, i.e. difficulty of discriminating caps in these hue bands, as demonstrated for normal trichromats (e.g. Laeng et al., 2007; Ao et al., 2019; Racheva, 2020; 2023), from pCPs' possible impairment of colour discrimination, we compared √PES medians for each hue band with those obtained for the control group (Racheva, 2020). (We are grateful to the authors for providing their data.) For seven hue bands, we found no statistically significant differences ($p>0.119$); for three hue bands, R–YR, GY–G and P–PR, √PES for pCPs were significantly lower ($p\leq0.04$), which could be accounted for by a lower illumination (285–295 lux) in (Racheva, 2020).

Further scrutiny of individual data (Table S2, Appendix 1) hints that in cases with small PES elevation, colour confusion is mainly observed in the G–BG and BG–B bands (Figure 1d). In comparison, in cases of slightly higher PES (Figure 1e, f), errors in the green-blue region are complemented by relatively small error "peaks" in the B–PB and RP–R bands. Finally, in more severe cases with the highest PES (Figure 1g, h), the pattern of errors is diffuse.

Figure 3
√PES measures for the post-COVID observers in ten specified hue bands

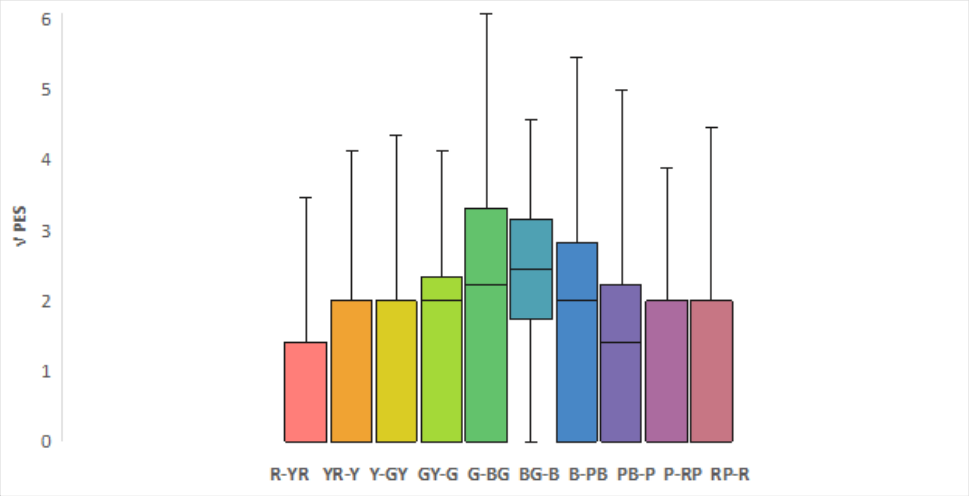

Note. *Boxplots represent the interquartile range; horizontal lines indicate medians (otherwise are equal to 0) and whiskers the outliers below the 1st quartile (BG–B band) or above the 3rd quartile for the other bands.*

We also explored √PES values for each of the ten hue bands as a function of the time elapsed after the participant's recovery but no statistically significant correlations were found (Table S3).

Colour discrimination along the B–Y and R–G axes

Figure 4a presents pCPs' data partitioned into √PES scores along the B–Y and R–G axes. It shows that √B–Y (mdn = 4.00, sIQR = 1.42) is significantly higher than √R–G (mdn = 3.16, sIQR = 1.35; $Z = -3.761$, $p<0.001$). The observed prevalence of B–Y errors is similar to the tendency reported for normal trichromats, both for younger and older observers (Beirne et al., 2008). The present means of √B–Y (4.09 ± 2.33) and √R–G (3.34 ± 2.11) are comparable to respective values, 4.04 ± 1.66 and 3.51 ± 1.97, obtained at 1000 lux (Woo & Lee, 2002).

We stratified √B–Y, √R–G and their difference according to participants' age groups, as shown in Table 2. It is apparent that, compared to means in Smith et al. (1985), for all age groups √B–Y and √R–G of pCPs are higher and the difference is greater.

Table 2

Mean √PES along the B–Y and R–G axes, and their difference for post-COVID participants, stratified for age groups, in comparison with Smith et al.'s (1985) means for normal trichromats

Age group	Post-COVID participants			Smith et al. (1985)		
(years)	√B–Y	√R–G	Diff.	√B–Y	√R–G	Diff.
15–19	+2.33	-1.59	+0.74	-	-	-
20–29	+4.35	-3.91	+0.44	+2.3	-3.3	-0.5
30–39	+4.27	-3.69	+0.57	+2.8	-2.8	+0.0
40–49	+4.09	-3.04	+1.04	+3.5	-2.1	+0.7
50–59	+4.16	-2.81	+1.35	+4.1	-1.5	+1.3
60–69	+5.61	-4.31	+1.30	-	-	-

We also explored whether for pCPs the √B–Y and √R–G difference reduced with the elapsed post-illness time. The correlation was not significant: $r = 0.1324$, $p = 0.251$: for a great participant majority the B–Y errors prevail, regardless of the number of days elapsed after the illness (Figure 4b).

Figure 4

√PES along the B–Y and R–G axes for post-COVID participants

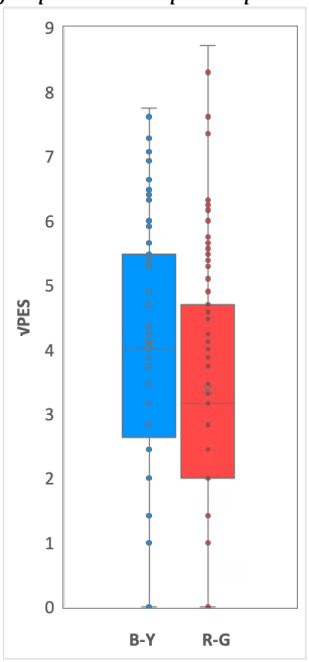

(a)

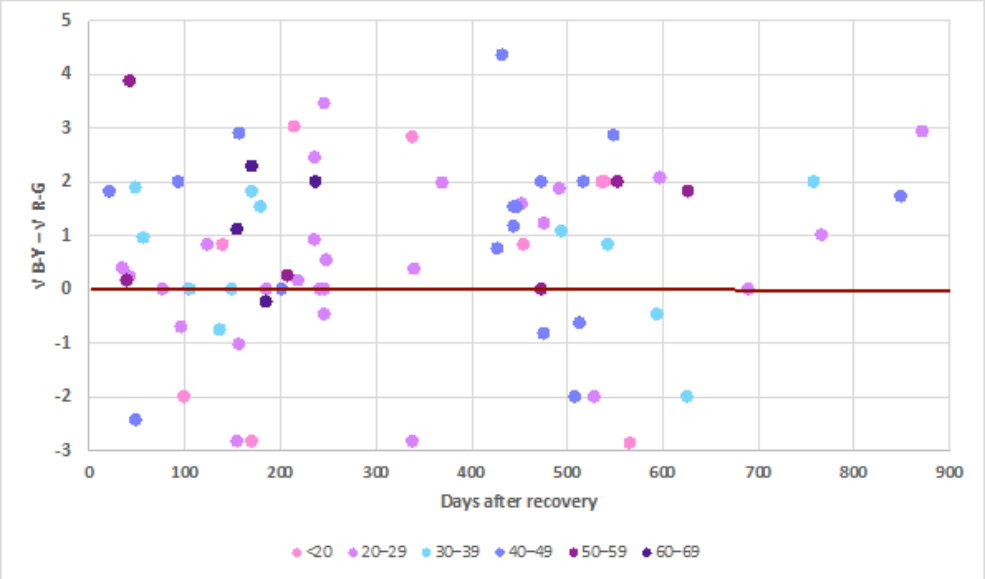

b

Note. *(a) Boxplots show the interquartile range of* $\sqrt{B–Y}$ *and* $\sqrt{R–G}$*; whiskers indicate the values beyond the range*; (b)* $\sqrt{B–Y} - \sqrt{R–G}$ *difference as a function of the time (days) elapsed after the recovery. Zero difference is indicated by a solid horizontal line. Colour-coded is participant's age group.*

Colour discrimination in different hemispheres of the FM-100 diagram

Figure S2 in Supplementary Materials presents √PES for pCPs for different FM-100 hemispheres. Figure S2a shows that colour discrimination was lower in the BG–B–PB–RP–RP gamut (right hemisphere) than in the R–YR–Y–GY–G gamut (left hemisphere): $Z = -4.144$, $p < 0.001$. Also, as expected (Figure 1a, b), Figure S2b shows that discrimination is lower in the green–blue (G–B) gamut (lower hemisphere) compared to the red–yellow (R–Y) gamut (upper hemisphere): $Z = -7.049$, $p<0.001$. More frequent confusions in the G–B range, i.e. √G–B – √R–Y difference, persist regardless of the time lapse after the participant's recovery ($r = -0.0529$, $p = 0.6471$), as illustrated by Figure S2c, where almost all points for individual observers lie above the zero line.

Vingrys and King-Smith's moment-of-inertia Vector Analysis

Applying the Vingrys & King-Smith (1988) vector analysis, for each pCP we estimated the Confusion index (*C-index*), or severity of CV impairment, Selectivity index (*S-index*), the amount of polarity in a cap arrangement, and the axis of confusion (*Angle*), which identifies the type of the colour defect. All individual participants' indices are presented in Table S4.

For the whole participant sample, the C-index highly correlated with √TES: ρ = 0.972 (p<0.001); the correlation of the S-index with √TES was medium: ρ = 0.421 (p <0.001); there was no significant association of √TES and the Angle: ρ = 0.101 (p = 0.381). We therefore agree with Bassi et al. (1993) that TES and the C-index are likely providing the same information.

Individual observers' C-index and S-index, as a function of the Angle, are shown as polar plots in Figure 5a, b. We start with considering the Angle index. Figure 5c indicates that for the overwhelming majority of pCPs (N = 72) the Angle was positive and ranged between 38°–88°, with mean 59.1°, i.e. very close to the 62.0° value reported for normal trichromats who made no errors in the D-15 test (Vingrys & King-Smith, 1988).

We also observe that for five pCPs, the Angle is negative. For four of these (#8, 10, 15, 71), the Angle >(–70°), characteristic for a tritan deficit (Vingrys & King-Smith, 1988; Bassi et al., 1993), and varies between (–77.7°) and (–84.2°). These Angle values are comparable with those of a patient with optic atrophy, OAB (–80.8°) and with mean Angle (–82.8°) for four congenital tritans (Vingrys & King-Smith, 1988). Descriptive statistics of FM-100 performance of the 'negative-Angle' pCPs is shown in Table S5. For comparison, also shown are corresponding means for other pCPs (N = 72) whose Angle values are positive.

Figure 5

The Vingrys and King-Smith indices for post-COVID participants; in (a) and (b), numbers indicate participant's ID

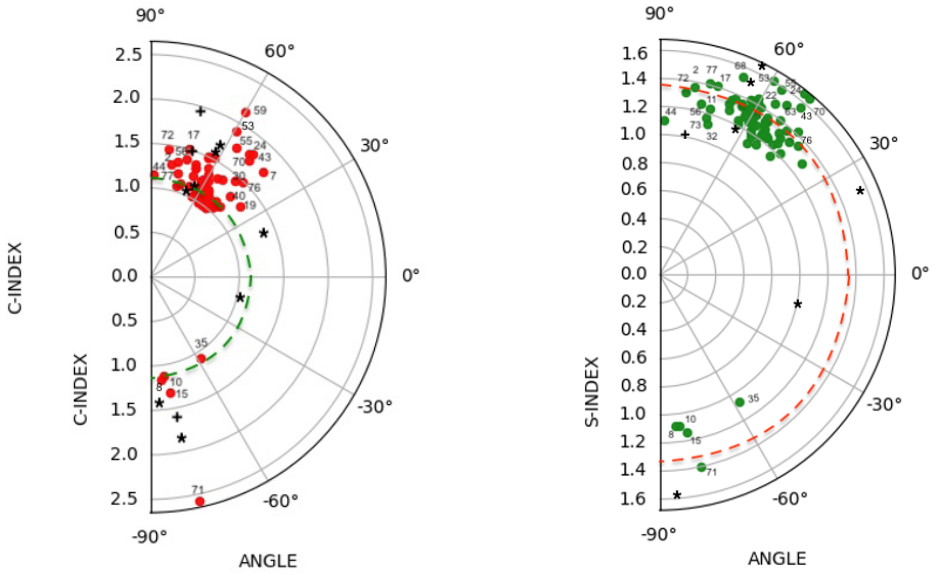

(a) (b)

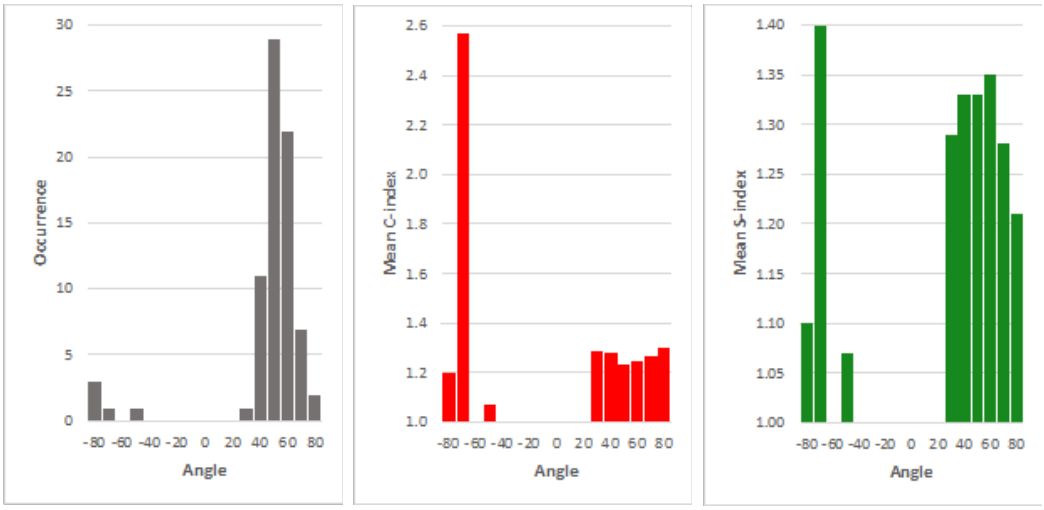

(c)

Note. *(a) C-index as a function of the Angle (red points); green dashed line indicates the cut-off value, C = 1.12, estimated for Caucasian normal trichromats (Dain et al., 2004). (b) S-index as a function of the Angle (green points); red dashed line indicates the cut-off value, S = 1.38, estimated for no-error normal trichromats (Vingrys & King-Smith, 1988). For comparison also shown are indices for normal trichromats, who made errors (*), and observer(s) with acquired colour vision loss (+) (Vingrys & King-Smith, 1988). (c) Left: Histogram of the distribution of the Angle, and distribution of the C-index (middle) and S-index (right) as the function of the Angle. (Note the difference in the y-axis scale across graphs).*

The distribution of the C-index (severity) for pCPs, as the function of the Angle, is shown in Figure 5c (middle). The C-index ranged between 1.0 (perfect cap arrangement; #18) and 2.57 (#71). Notably, among the 'positive-Angle' participants (N = 72), for 31 $C \leq 1.12$, which we adopted as the cut-off criterion (Table S5), based on the C-index mean value obtained for Caucasian normal trichromats with light irides (Dain et al., 2004). However, for 41 observers the C-index >1.12 and varied between 1.14–2.14 (mean 1.40). For 4 (out of 5) 'negative-Angle' observers, the C-index varied between 1.07–1.32. The highest C-index, 2.57 (#71; Figure 1h) is comparable to that for four tritans, 2.70, and somewhat lower than the C-index for a patient with optic atrophy (OAA), 3.0 (Vingrys & King-Smith, 1988).

Figure 5c (right) shows distribution of pCPs' S-index, which ranges between 1.07–1.65. Among the 'positive-Angle' participants (N = 72), for the majority (N = 41) with C>1.12, the cut-off criterion, mean S-index is 1.37 (Table S5), i.e. comparable to S = 1.38

for no-error normal trichromats (Vingrys & King-Smith, 1988), i.e. indicating non-polar cap arrangements. For the four 'negative-Angle' observers, the S-index varies between 1.07–1.14. Participant #71's S-index, 1.40, is close to the upper limit, S = 1.38; it is similar to S-indices of the majority of glaucoma patients (Bassi et al., 1993) and definitely lower than mean S-index for four tritans, 3.94, or a tritanope's S-index, 4.74 (Vingrys & King-Smith, 1988).

Clusters of post-COVID participants based on FM-100 performance indices

The outcome of the hierarchical cluster analysis (Figure 6) visualizes, as a 2D map, similarities of FM-100 performance, TES and the three moment-of-inertia parameters, of individual pCPs. Detailed numerical information on performance of the participants performance constituting each cluster is provided in Table S6.

Figure 6

A 2D map illustrating similarity of FM-100 performance of post-COVID participants

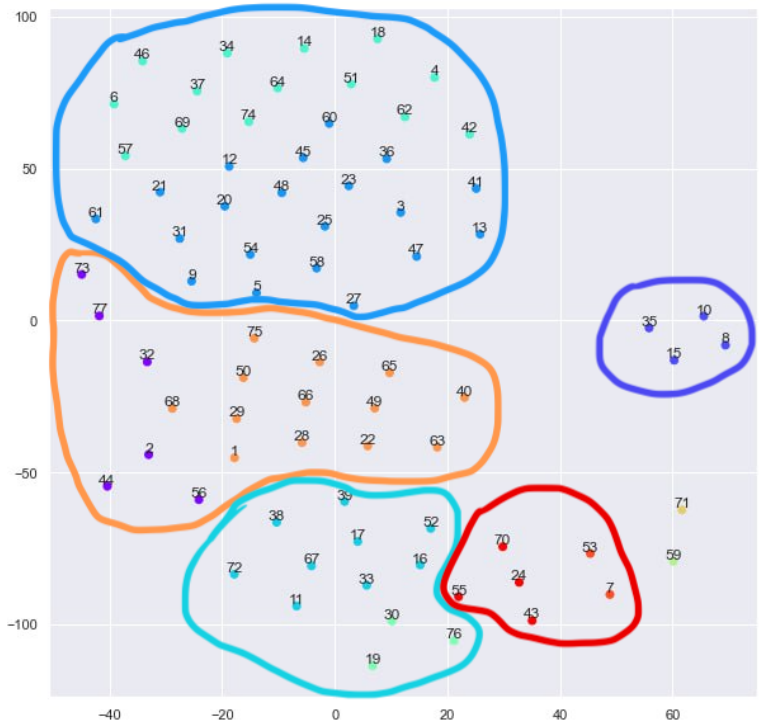

Note. *Proximity measures are based on TES and the three vector analysis parameters. (Sub) clusters are colour-coded in the program outcome. Data-points are accompanied by participants' ID.*

As is prompted by Figure 6 and Table S6, FM-100 performance of almost all pCPs is encompassed by five clusters:

- The top cluster includes cases of *superior discrimination* (N = 34), with TES<28, pCPs' median. In the "turquoise" sub-cluster (N = 14), the "severity" parameters are very low: TES = 0–8, C = 1.00–1.09; in the "blue" sub-cluster (N = 20), the corresponding parameters are slightly higher: TES = 8–24, C = 1.01–1.17.
- The middle cluster is constituted by cases of *average discrimination* (N = 19), with TES mostly between 50%–80%. In the "hazel" sub-cluster (N = 13), TES varies between 28–44; however, C = 1.17–1.34, i.e. C>1.12. In the "violet" sub-cluster (N = 6), TES is slightly higher, 16–68, as are the C = 1.07–1.49. In both sub-clusters, in a few cases S>1.38.
- The bottom cluster encompasses, too, cases of *average discrimination* (N = 12; "cyan" and "light green") with TES = 52–72, slightly higher C = 1.29–1.53, and some *blue-yellow error polarity* reflected S = 1.24–1.42.
- The abutting "red" cluster (N = 6) denotes cases of *poor discrimination*: TES = 84–116, C = 1.72–1.90, S = 1.35–1.65.
- A small "dark blue" cluster (N = 4) includes cases with negative Angle indicating a tritan defect; the discrimination is good or average (TES = 20–56); C = 1.07–1.32, though in two cases C>1.12; S = 1.07–1.14 indicating no error polarity.

The two cases, #59 and #71, unambiguously manifest CV loss, both with the highest √B-Y. For #59, TES = 176, C = 2.14, S = 1.26. Colour discrimination of #71 is affected most in the sample, reflected by TES = 212, C = 2.57, S = 1.40 and a negative Angle.

Discussion

We have investigated colour discrimination in pCPs, using the FM-100 to assess whether an acquired CV deficiency existed and if that was the case, the deficiency's severity and type. For the whole sample, mean TES = 38.1 ± 37.8 is comparable to normal trichromats' mean 34.1 ± 28 (Laeng et al., 2007) or 37.4 (at 275-lux illumination) (Mahon & Vingrys, 1995), and lower than 43 ± 3 (Shepherd, 2005), 45.8 (Cranwell et al., 2015) or 62.1 (Verriest, 1963). Mean √TES was 5.52 ± 2.77, slightly higher than 5.48 ± 2.27 for Caucasian observers tested at 1000 lux (Woo, & Lee, 2002). It is also higher than √TES for observers with varying iris colour – dark (5.04 ± 1.76), medium (4.59 ± 1.82) or light (4.18 ± 1.64) respectively (250-lux testing illumination) (Dain et al., 2004).

For age groups, there was generally a good correspondence between pCPs' mean √TES and earlier data sets for normal trichromats (Verriest et al., 1982; Roy et al., 1991; Kinnear & Sahraie, 2002) (Table 1). Beyond mean √TES, rather unexpectedly, we found that CV was affected in considerable pCP subsamples of the 20-29 y.o. and 30-39 y.o. groups (Figure S1), whose scores were elevated compared to the corresponding normal trichromats' means (Verriest et al., 1982), although in the latter the FM-100 was administered at 200-lux illuminance, which implies decreased chromatic sensitivity (Knoblauch et al., 1987).

The FM-100 diagram presenting pCPs' mean error scores for individual caps (Figure 1a,b) shows a minor but definite peak in the G–BG–B–PB region and another minor crest in the RP–R region. This observation is buttressed by the finding that discrimination is lower in the G–B gamut compared to the R–Y gamut (Figure S2). Critically, notwithstanding mean √TES for all pCPs' age groups comparable to those in previous studies (Verriest et al., 1982; Roy et al., 1991; Kinnear & Sahraie, 2002), √B–Y and √R–G were higher and the (√B–Y – √R–G) difference was greater compared to the means obtained at 170-lux illuminance by Smith et al. (1985) (Table 2) confirming, cross-sectionally, a mild tritan deficiency in pCPs. Furthermore, the B–Y errors prevail in the great majority of participants, regardless of the recovery time elapsed after the illness.

Notably, among pCPs we found a significant inter-individual variation, TES = 0–212 (Table S2, Appendix 1). Based on TES, the great majority of pCPs revealed either superior performance, 0≤TES≤24, below the median (Figure 1c), or average colour discrimination, 28≤TES≤84 (90th percentile; Figure 1d,e), while a minor subsample had poor discrimination (Figure 1f) or unambiguous CV loss (Figure 1g,h).

The Vingrys & King-Smith (1988) vector analysis provided additional information (Figure 5, Table S4) for a more precise estimation of severity and type of mild CV impairment in pCPs, who made errors. We adopted the conservative cut-off criterion, C = 1.12, mean C-index for Caucasian normal trichromats with light irides obtained using the FM-100 (Dain et al., 2004), rather than C = 1.60 recommended by Vingrys & King-Smith (1988) based on D-15 data; for the S-index, we applied the cut-off criterion, S = 1.38, as recommended in (Vingrys & King-Smith, 1988). The Vingrys & King-Smith (1988) analysis enabled us to identify 5 participants with a negative Angle indicating a tritan defect. Moreover, among the 'positive-Angle' participants (N = 72), in many cases (N = 41) the C-index, 1.14–2.14, exceeded the cut-off criterion (Table S5), pointing to a subtle colour discrimination abnormality.

Cluster analysis, based on both TES and the Vingrys & King-Smith (1988) indices, allowed a greater scrutiny of subsamples of pCPs with regard to colour discrimination and, particularly, the kind of mild CV impairment (Figure 6, Table S6). The analysis confirmed that a substantial number of pCPs (N = 34) demonstrated *superior* performance (cluster 1).

Importantly, it revealed variation among pCPs with *average* colour discrimination (N = 31), with clusters (2) and (3) differing not as much in TES range but in the pattern of errors pointing to subtle tritan defects, or Type III acquired colour deficiency, according to Verriest (1963). Cluster (2) discerns cases with the *monopolar blue* error pattern (Figure 1d), or Type III mild solely 'blue' colour deficiency, in accord with a revised classification of Pokorny & Smith (1986). In comparison, cluster (3) comprises cases of mild tritan defects with the error pattern along the *blue-yellow* axis (Figure 1e).

Still another minor subsample (cluster 4, N = 6) manifested *poor discrimination* (>95th percentile; Figure 1f) classified as Type III moderate defect (Pokorny & Smith, 1986). It is noteworthy that the cases of the "light green" sub-cluster are characterised by a *diffuse*

error pattern; the Angle, 38°–46°, deviates from the 62.0°, mean value for no-error normal trichromats (Vingrys & King-Smith, 1988). We observe that similar Angle range is characteristic for protanomals (Vingrys & King-Smith, 1988) and some glaucoma patients (Bassi et al., 1993). In the abutting #59 case (Figure 1g) all severity indices are still greater and the error pattern is diffuse, thus, unambiguously indicating CV loss.

Finally, cluster (5) comprises pCPs with negative Angle (N = 4). For 3 of these, the C-index exceeded the cut-off criterion (Table S5). For the adjoining negative-Angle case #71, the most severe in the sample (Figure 1h), all severity indices are above normal and polarity indices indicate a tritan defect.

We address the finding that mean √TES of pCPs, estimated at ca. 1000 lux, appears to be comparable to mean √TES obtained at lower photopic levels (200 lux Verriest et al., 1982)) or higher than these (250 lux (Dain et al., 2004)); also, mean √B–Y and √R–G are greater than the corresponding values assessed at 170 lux (Smith et al., 1985). According to Verriest (1964, cit. in (Dain et al., 2004)), in pCPs this could be the sign of 'mesopization' of colour discrimination attributed to reduction in luminosity efficiency. The FM-100 performance, specifically, that reveals a mild acquired deficiency is likened to that of normal trichromats at lower illuminance levels, or colour discrimination loss that resembles its senile decrease and the congenital tritan type (Verriest, 1963; Knoblauch et al., 1987). Lakowski (1966) attributed it to reduction in luminosity efficiency of the retinal receptor system; Dain et al. (2004) conjectured that 'mesopization', or tritan deficiency, could arise without postulating specific damage to the blue-yellow system.

General "darkening" of perceived colours by pCPs was hinted by our recent colour-naming study (Griber & Paramei, 2022a; 2022b): supposedly, perceived colour dimming translated into a greater prevalence than in pre-COVID controls of the terms 'brown' and 'grey', and higher frequency of achromatic modifiers 'dark' and 'dirty', which were elicited particularly frequently in combination with 'green', 'blue', and 'purple'.

One may query loci and mechanism(s) that underlie mild colour discrimination impairment in about half of those who recovered from COVID-19. Leaning on our findings of increased naming "darkening" of colours by pCPs (Griber & Paramei, 2022a; 2022b), we pondered that it might manifest an accelerated brunescence of the crystalline lens, resulting in an increased absorption of light, in particular, in the blue and purple gamut. Further, if lens brunescence has developed over a short illness time span, the affected colour perception could not have been compensated (at the level of colour naming), since the compensation process is being developed across the age span (Hardy et al., 2005). However, the improvement of colour discrimination with increasing post-illness time lapse, found in the present study (Figure 2), suggests that that the lens brunescence hypothesis is to be rejected.

Notably, a case of sudden (transient) darkening of the visual field following COVID-19 vaccination was reported (Santovito & Pinna, 2021) and attributed to hypoperfusion (reduced vascular supply) of either the retina, or optic nerves, or parts of the visual pathway extending to the visual cortices (Eleiwa et al., 2021). A COVID-19-caused reduction of

blood/oxygen supply at the retinal and/or post-retinal stages of the visual system is a more parsimonious explanation. This hypothesis is plausible in view of pCPs' mild and moderate Type III defects, identified in the present study, that are characteristic of vascular retinopathies and optic atrophy (Pokorny & Smith, 1986; Simunovic, 2016). Indeed, retinal changes and alterations of retinal vasculature in response to oxygen decrease (Invernizzi et al., 2020), and disorder of retinal capillaries (Giacuzzo et al., 2022) were reported in those exposed to coronavirus. Relevant are in this regard findings in two studies that applied the FM-100 and reported mild hypoxia-induced CV impairment, with reduced discrimination along the blue-yellow axis (Smith et al., 1976) or a generalised depression of both blue-yellow and red-green sensitivity (Vingrys & Garner, 1987).

We would like to remark that in our colour-naming study of pCPs (Griber & Paramei, 2022a; 2022b) we found that, along with "darkening", these respondents also revealed an increased frequency of 'pale'-, 'dull'- and 'pastel'-modifiers, which hint at desaturation of perceived colours. Notably, comments that colours looked duller, paler or less glossy were recorded from patients with optic neuritis (Mullen & Plant, 1987). Also, the pCPs' "desaturation" naming alludes to the finding for migraine patients, whose settings of colours were consistently paler than in controls (Shepherd, 2005).

We suppose that joint "darkening" and "desaturation" in the colour-naming pattern of pCPs may be indicative of an affected processing of colour and luminance contrast. As conjectured by Bimler et al. (2009), at a hypothetical stage in the visual system the two post-receptoral opponent systems feed into the channel that combines Brightness and Chrominance (saturation) information, whereby a depressed input signal to this channel produces black induction and desaturation of perceived colours, which appear matt and dull. One can only speculate about the visual system stage affected by coronavirus.

Mullen and Plant (1987) assumed that the deficits of perceived saturation in patients with optic neuritis were caused by the affected ganglion cells with small diameter axons (projecting to the parvocellular layers of the lateral geniculate nucleus), which respond to colour differences. Shepherd (2005) considers that migraine participants' perception of colours as paler likely arises at a site in the visual pathways proximal to the retina, but could arise throughout the visual pathway or at one of many stages within it. She argues that specific subjective desaturation of the S-cone colours (purple, yellow) "suggests a stage or stages before the signals from the colour opponent pathways combine" (Shepherd, 2005, p. 421). This contention is echoed by Mahon & Vingrys' (1996) view that disease-related desaturation may occur at any pre-cortical level or at multiple levels within the visual system. Their model (Mahon & Vingrys', 1996) supports clinical observations of saturation losses occurring early in disease; the authors argue that saturation discrimination thresholds may yield added clinical information in detecting dysfunction.

Cross-sectionally, we found a weak negative correlation between pCPs' √TES and the elapsed recovery time (Figure 2). In our cautiously optimistic forecast of further improvement of colour discrimination with increased post-illness period we are encouraged by ophthalmological reports that most cases of dyschromatopsia later

reversed (Giacuzzo et al., 2022; Richardson-May et al., 2022); also, medium-term findings of subtle retinal changes suggested a good visual prognosis in patients recovering from COVID-19 (Costa et al., 2021).

Our study presents some limitations. Two oldest age group were represented by only a few participants. Further, in relation to the elapsing recovery period, TES was assessed cross-sectionally; thus, the estimated negative correlation is indicative rather than decisive with regard to potential colour discrimination improvement.

In our final remark, we note that CV loss identified post-COVID in ophthalmological examination using the Ishihara test (Clarke et al., 2021; Giacuzzo et al., 2022; Nagaratnam et al., 2022; Richardson-May et al., 2022) conceivably captured moderate and/or relatively severe CV loss. Intended to diagnose red-green deficiencies, the Ishihara test cannot reveal subtle tritan defects (Lakowski, 1969), as those that we identified in more than half of pCPs by employing the FM-100. We are aware that in routine clinical practice, use of the FM-100 is limited by its relatively long test times, and complicated and time-consuming analysis. The Ishihara test could be complemented by an arrangement test in cases, where detection and diagnosis of subtle CV defects is reasonable, as suggested by Lakowski (1969). As a proxy, the Lanthony D-15 desaturated test, which has predictive ability for assessing the severity of CV loss in patients (Bassi et al., 1993), can be administered at a fraction of the time of the FM-100.

Acknowledgements

The authors are indebted to Margarita Zlatkova and Kalina Racheva for providing individual data of FM-100 partial error scores for their control group of normal trichromats. We thank Tatjana Samoilova for re-writing the Vingrys & King-Smith (1988) program for calculation of the moment of inertia, from Basic in Excel VBA, as well as for her help in data analysis. Support of Alexei Delov and Karina Zygankova in data processing is gratefully appreciated. The authors thank all participants for their time and good will. We are grateful David Bimler for valuable comments on and proofreading of an earlier version of the manuscript.

References

Ao, M., Li, X., Qiu, W., Hou, Zh., Su, J., & Wang, W. (2019). The impact of age-related cataracts on colour perception, postoperative recovery and related spectra derived from test of hue perception. *BMC Ophthalmology, 19*, 56. https://doi.org/10.1186/s12886-019-1057-6

Barton, F. B., Fong, D. S., & Knatterud, G. L. (2004). Classification of Farnsworth-Munsell 100-hue test results in the early treatment diabetic retinopathy study. *American Journal of Ophthalmology, 138*(1), 119–124 https://doi.org/10.1016/j.ajo.2004.02.009

Bassi, C. J., Galanis, J. C., & Hoffman, J. (1993). Comparison of the Farnsworth-Munsell 100-Hue, the Farnsworth D-15, and the L'Anthony D-15 desaturated color tests. *Archives of Ophthalmology, 111*(5), 639–641. https://doi.org/10.1001/archopht.1993.01090050073032

Beirne, R. O., McIlreavy, L., & Zlatkova, M. B. (2008). The effect of age-related lens yellowing on Farnsworth-Munsell 100 hue error score. *Ophthalmic and Physiological Optics, 28*(5), 448–456. https://doi.org/10.1111/j.1475-1313.2008.00593.x

Bento-Torres, N. V. O., Rodrigues, A. R., Côrtes, M. I. T., Bonci, D. M. O., Ventura, D. F., & Silveira, L. C. L. (2016). Psychophysical evaluation of congenital colour vision deficiency: Discrimination between protans and deutans using Mollon-Reffin's ellipses and the Farnsworth-Munsell 100-hue test. *PLoS ONE, 11*(4), e0152214. https://doi.org/10.1371/journal.pone.0152214

Bimler, D. L., Paramei, G. V., & Izmailov, C. A. (2009). Hue and saturation shifts from spatially induced blackness. *Journal of the Optical Society of America A, 26*(1), 163–172. https://doi.org/10.1364/JOSAA.26.000163

Bimler, D. L., Paramei, G. V., Feitosa-Santana, C., Oiwa, N. N., & Ventura, D. F. (2014). Saturation-specific pattern of acquired colour vision deficiency in two clinical populations revealed by the method of triads. *Color Research and Application, 39*(2), 125–135. https://doi.org/10.1002/col.21794

Birch, J. (2001). *Diagnosis of defective colour vision* (2nd ed.). Butterworth Heinemann.

Birch, J. M., Chisholm, I. A., Kinnear, P., Marre, M., Pinckers, A. J. L. G., Pokorny, J., Smith, V. C., Verriest, G. (1979). Acquired color vision defects. In J. Pokorny, V. C. Smith, G. Verriest, & A. J. L. G. Pinckers (Eds.), *Congenital and Acquired Color Vision Defects* (pp. 282–284). Grune and Stratton Inc.

Castelo-Branco, M., Faria, P., Forjaz, V., Kozak, L.R., & Azevedo, H. (2004). Simultaneous comparison of relative damage to chromatic pathways in ocular hypertension and glaucoma: Correlation with clinical measures. *Investigative Ophthalmology & Visual Science, 45*(2), 499–505. https://doi.org/10.1167/iovs.03-0815

Clarke, K. M., Riga, V., Shirodkar Al., & Meyer, J. (2021). Proning related bilateral anterior ischaemic optic neuropathy in a patient with COVID-19 related acute respiratory distress syndrome. *BMC Ophthalmology, 21*, 276. https://doi.org/10.1186/s12886-021-02028-9

Costa, Í. F., Bonifácio, L. P., Bellissimo-Rodrigues, F., Rocha, E. M., Jorge, R., Bollela, V. R., & Antunes-Foschini, R. (2021). Ocular findings among patients surviving COVID-19. *Scientific Reports, 11,* 11085. https://doi.org/10.1038/s41598-021-90482-2

Cranwell, M. B., Pearce, B., Loveridge, C., & Hurlbert, A. C. (2015). Performance on the Farnsworth-Munsell 100-Hue Test is significantly related to nonverbal IQ. *Investigative Ophthalmology & Visual Science*, *56*(5), 3171–3178. https://doi.org/10.1167/iovs.14-16094

Dain, S. J. (2004). Clinical colour vision tests. *Clinical and Experimental Optometry, 87*(4-5), 276–293. https://doi.org/10.1111/j.1444-0938.2004.tb05057.x

Dain, S. J., Cassimaty, V. T., & Psarakis, D. T. (2004). Differences in FM100-Hue test performance related to iris colour may be due to pupil size as well as presumed amounts of macular pigmentation. *Clinical and Experimental Optometry, 87*(4–5), 322–325. https://doi.org/10.1111/j.1444-0938.2004.tb05061.x

Dain, S. J., Scase, M. O., & Foster, D. H. (1991). An assessment of the 'mesopization' model of blue-yellow colour vision defects. In B. Drum, J. D. Moreland, & A. Serra (Eds.), *Colour Vision Deficiencies X*, *Documenta Ophthalmologica Proceedings Series, 54* (pp. 187–197). Springer. https://doi.org/10.1007/978-94-011-3774-4_23

Eleiwa, T. K. Gaier, E. D., Haseeb, A., ElSheikh, R. H., Sallam, A. B., & Elhusseiny, A. M. (2021). Adverse ocular events following COVID-19 vaccination. *Inflammation Research, 70*, 1005–1009. https://doi.org/10.1007/s00011-021-01506-6

Esposito, T. (2019). An adjusted error score calculation for the Farnsworth-Munsell 100 Hue Test. *LEUKOS: The Journal of the Illuminating Engineering Society,* 15 (2–3), 195–202. https://doi.org/10.1080/15502724.2018.1514265

Farnsworth, D. (1943). The Farnsworth-Munsell 100-hue and dichotomous tests for color vision. *Journal of the Optical Society of America, 33*(10), 568–578.

Farnsworth, D. (1957). *The Farnsworth-Munsell 100-Hue Test for the Examination of Color Discrimination*: *Manual*. Munsell Color Company.

François, J., & Verriest, G. (1961). On acquired deficiency of colour vision, with special reference to its detection and classification by means of the tests of Farnsworth. *Vision Research, 1*(3–4), 201–219 https://doi.org/10.1016/0042-6989(61)90001-3

Gangaputra, S. S., & Patel, S. N. (2020). Ocular symptoms among nonhospitalized patients who underwent COVID-19 testing. *Ophthalmology*, *127*(10), 1425–1427. https://doi.org/10.1016/j.ophtha.2020.06.037

Giacuzzo, C., Eandi, C. M., & Kawasaki, A. (2022). Bilateral acute macular neuroretinopathy following COVID-19 infection. *Acta Ophthalmologica, 100*(2), e611–e612. https://doi.org/10.1111/aos.14913

Griber, Y. A., & Paramei, G. V. (2022a). Colour naming of post-COVID participants hints to "darkening" of perceived colour. In *Proceedings of the International Colour Association (AIC) Conference "Sensing Colour", 13th-16th June 2022, Toronto, Canada* (pp. 504–508). International Colour Association.

Griber, Y. A., & Paramei, G. V. (2022b). Postkovidnoe cvetovospijatie: Vlijanie Covid-19 na vybor cvetonaimenovanija [Post-COVID color perception: The impact of COVID-19 on color naming]. *Russian Psychological Journal, 19*(3), 21–40 (in Russian and English). https://doi.org/10.21702/rpj.2022.3.2

Gundogan, F. C., Tas, A., Altun, S., Oz, O., Erdem, U., & Sobaci, G. (2013). Color vision versus pattern visual evoked potentials in the assessment of subclinical optic pathway involvement in multiple sclerosis. *Indian Journal of Ophthalmology, 61*(3), 100–103. https://doi.org/10.4103/0301-4738.99842

Hardy, J. L., Frederick, C. M., Kay, P., & Werner, J. S. (2005). Color naming, lens aging, and grue: What the optics of the aging eye can teach us about color language. *Psychological Science, 16*(4), 321–327. https://doi.org/10.1111/j.0956-7976.2005.01534.x

Hart, W. M. Jr. (1987). Acquired dyschromatopsia. *Survey of Ophthalmology, 32*(1), 10–31. https://doi.org/10.1016/0039-6257(87)90070-1

Haseeb, A. A., Solyman, O., Abushanab, M. M., Abo Obaia, A. S., & Elhusseiny, A. M. (2022). Ocular complications following vaccination for COVID-19: A one-year retrospective. *Vaccines, 10*, 342. https://doi.org/10.3390/vaccines10020342

Invernizzi, A., Torre, A., Parrulli, S., Zicarelli, F., Schiuma, M., Colombo, V., Giacomelli, A., Cigada, M., Milazzo, L., Ridolfo, A., Faggion, I., Cordier, L., Oldani, M., Marini, S., Villa, P., Rizzardini, G., Galli, M., Antinori, S., Staurenghi, G., & Meroni, L. (2020). Retinal findings in patients with COVID-19: Results from the SERPICO-19 study. *EClinicalMedicine, 27,* 100550. https://doi.org/10.1016/j.eclinm.2020.100550

Kinnear, P. R. (1970). Proposals for scoring and assessing the 100 hue test. *Vision Research, 10*(5), 423–433. https://doi.org/10.1016/0042-6989(70)90123-9

Kinnear, P. R., & Sahraie, A. (2002). New Farnsworth-Munsell 100 hue test norms of normal observers for each year of age 5-22 and for age decades 30–70. *British Journal of Ophthalmology, 86*(12), 1408–1411. https://doi.org/10.1136/bjo.86.12.1408

Knoblauch, K. (1987). On quantifying the bipolarity and axis of the Farnsworth-Munsell 100-hue test. *Investigative Ophthalmology & Visual Science, 28*(4), 707–710.

Knoblauch, K., Saunders, F., Kusuda, M., Hynes, R., Podgor, M. Higgins, K. E., & de Monasterio F. M. (1987). Age and illuminance effects in the Farnsworth-Munsell 100-hue test. *Applied Optics, 26*(8), 1441–1448. https://doi.org/10.1364/AO.26.001441

Köllner, H. (1912). *Die Störungen des Farbensinnes, ihre klinische Bedeutungen und ihre Diagnose*. Karger.

Laeng, B., Brennen, T., Elden, Å., Paulsen, H. G., Banerjee, A., & Lipton, R. (2007). Latitude-of-birth and season-of-birth effects on human color vision in the Arctic. *Vision Research*, *47*, 1595–1607. https://doi.org/10.1016/j.visres.2007.03.011

Lakowski, R. (1966). A critical evaluation of colour vision tests. *British Journal of Physiological Optics, 23*(3),186–209.

Lakowski, R. (1969). Theory and practice of colour vision testing: A review. Part 2. *British Journal of Industrial Medicine,* 26, 265–288. http://dx.doi.org/10.1136/oem.26.4.265

Mahon, L. E., & Vingrys, A. J. (1995). Scoring the Farnsworth-Munsell 100-Hue for vocational guidance. *Optometry and Vision Science, 72*(8), 547–551.

Mahon, L. E., & Vingrys, A. J. (1996). Normal saturation processing provides a model for understanding the effects of disease on color perception. *Vision Research, 36*(18), 2995–3002. https://doi.org/10.1016/0042-6989(95)00319-3

Mäntyjärvi, M. (2001). Normal test scores in the Farnsworth–Munsell 100 hue test. *Documenta Ophthalmologica, 102*, 73–80. https://doi.org/10.1023/A:1017553532092

Ménage, M. J., Papakostopoulos, D., Hart, J. C. D., Papakostopoulos, S., & Gogolitsyn, Yu. (1993). The Farnsworth-Munsell 100 hue test in the first episode of demyelinating optic neuritis. *British Journal of Ophthalmology*, *77*, 68–74. http://dx.doi.org/10.1136/bjo.77.2.68

Mullen, K. T., & Plant, G. T. (1987). Threshold and suprathreshold deficits in color vision in optic neuritis. In G. C. Woo (Ed.), *Low Vision* (pp. 29–44). Springer. https://doi.org/10.1007/978-1-4612-4780-7_3

Nagaratnam, S. A., Ferdi, A. C., Leaney, J., Lee, R. L. K., Hwang, Y. T., & Heard, R. (2022). Acute disseminated encephalomyelitis with bilateral optic neuritis following ChAdOx1COVID-19 vaccination. *BMC Neurology, 22*, 54. https://doi.org/10.1186/s12883-022-02575-8

Nagy, Z. Z. (2020). Ophthalmic signs and complications of the COVID-19 infection. *Developments in Health Sciences, 3*(4), 79–82. https://doi.org/10.1556/2066.2021.40001

Paramei, G. V., & Bimler, D. L. (2019). Color vision testing. In R. Shamey (Ed.), *Encyclopedia of Color Science and Technology* (2nd ed.). Springer, https://link.springer.com/referenceworkentry/10.1007/978-3-642-27851-8_374-2

Pokorny, J., & Smith, V. C. (1986). Eye disease and color defects. *Vision Research, 26*(9), 1573–1584. https://doi.org/10.1016/0042-6989(86)90176-8

Racheva, K., Totev, Ts., Natchev, E., Bocheva, N., Beirne, R., & Zlatkova, M. (2020). Color discrimination assessment in patients with hypothyroidism using the Farnsworth-Munsell 100 hue test. *Journal of the Optical Society of America A, 37*(4), A18–A25. https://doi.org/10.1364/JOSAA.382390

Racheva, K., Totev, Ts., Natchev, E., Bocheva, N., Beirne, R., & Zlatkova, M. (2023). Elimination of the color discrimination impairment along the blue–yellow axis in patients with hypothyroidism after treatment with levothyroxine as assessed by the Farnsworth–Munsell 100 hue test. *Journal of the Optical Society of America A, 40*(3), A26–A32 https://doi.org/10.1364/JOSAA.476139

Raman, R., Verma, A., Srinivasan, S., & Bhojwani, D. (2018). Partial reversal of color vision impairment in type 2 diabetes associated with obstructive sleep apnea. *GMS Ophthalmology Cases, 8*, Doc05. https://doi.org/10.3205/oc000087

Richardson-May, J., Purcaru, E., Campbell, C., Hillier, C., & Parkin, B. (2022). Guillain-Barré Syndrome and unilateral optic neuritis following vaccination for COVID-19: A case report and literature review. *Neuro-Ophthalmology*, *46*(6), 413–419. https://doi.org/10.1080/01658107.2022.2048861

Roy, M. S., Podgor, M. J., Collier, B., & Gunkel, R. D. (1991). Color vision and age in a normal North American population. *Graefe's Archive for Clinical and Experimental Ophthalmology = Albrecht von Graefes Archiv für klinische und experimentelle Ophthalmologie, 229*(2), 139–144. https://doi.org/10.1007/BF00170545

Santovito, L. S., & Pinna, G. (2021). Acute reduction of visual acuity and visual field after Pfizer-BioNTech COVID-19 vaccine 2nd dose: a case report. *Inflammation Research*, *70*, 931–933. https://doi.org/10.1007/s00011-021-01476-9

Schneck, M. E., & Haegerstrom-Portnoy, G. (1997). Color vision defect type and spatial vision in the optic neuritis treatment trial. *Investigative Ophthalmology & Visual Science, 38*, 2278–2289.

Shepherd, A J. (2005). Colour vision in migraine: selective deficits for S-cone discriminations. *Cephalalgia, 25*(6), 412–423. https://doi.org/10.1111/j.1468-2982.2004.00831.x

Shoji, T., Sakurai, Y., Sato, H., Chihara, E., & Takeuchi, M. (2011). Do type 2 diabetes patients without diabetic retinopathy or subjects with impaired fasting glucose have impaired colour vision? The Okubo Color Study Report. *Diabetic Medicine, 28*(7), 865–871 https://doi.org/10.1111/j.1464-5491.2011.03290.x

Simunovic, M. P. (2016). Acquired color vision deficiency. *Survey of Ophthalmology, 61*(2), 132–155. https://doi.org/10.1016/j.survophthal.2015.11.004

Smith, V. C., Ernest, T. J., & Pokorny, J. (1976). Effect of hypoxia on FM100-Hue test performance. In G. Verriest (Ed.), *Modern Problems in Ophthalmology*, *17* (pp. 248–256). Karger.

Smith, V. C., Pokorny, J., & Pass, A. S. (1985). Color axis determination on the Farnsworth-Munsell 100-hue test. *American Journal of Ophthalmology, 100*(1), 176–182. https://doi.org/10.1016/s0002-9394(14)75002-0

Verriest, G. (1963). Further studies on acquired deficiency of color discrimination. *Journal of the Optical Society of America, 53*(1), 185–195. https://doi.org/10.1364/JOSA.53.000185

Verriest, G., Van Laethem, J., & Uvijls, A. (1982). A new assessment of the normal ranges of the Farnsworth-Munsell 100-Hue test scores. *American Journal of Ophthalmology, 93*(5), 635–642. https://doi.org/10.1016/s0002-9394(14)77380-5

Vingrys, A. J., & Garner, L. F. (1987). The effect of a moderate level of hypoxia on human color vision. *Documenta Ophthalmologica, 66*, 171–185. https://doi.org/10.1007/BF00140454

Vingrys, A. J., & King-Smith, P. E. (1988). A quantitative scoring technique for panel tests of color vision. *Investigative Ophthalmology & Visual Science, 29*(1), 50–63.

Ward, Jr. J. H. (1963). Hierarchical grouping to optimize an objective function. *Journal of the American Statistical Association, 58*(301), 236–244. https://doi.org/10.1080/01621459.1963.10500845

Woo, G. C., & Lee, M.-h. (2002). Are ethnic differences in the F-M 100 scores related to macular pigmentation? *Clinical and Experimental Optometry, 85*(6), 372–377. https://doi.org/10.1111/j.1444-0938.2002.tb02388.x

X-Rite. Farnsworth Munsell 100 Hue Scoring Software webpage. (2024b). https://www.xrite.com/categories/visual-assessment-tools/fm-100-hue-scoring-system

X-Rite. Farnsworth Munsell 100 Hue Test webpage. (2024a). https://www.xrite.com/categories/visual-assessment-tools/fm-100-hue-test

Yüksel, B., Bıçak, F., Gümüş, F., & Küsbeci, T. (2022). Non-arteritic anterior ischaemic optic neuropathy with progressive macular ganglion cell atrophy due to COVID-19. *Neuro-Ophthalmology, 46*(2), 104–108. https://doi.org/10.1080/01658107.2021.1909075

Supplementary Materials

The following supporting information can be downloaded at: https://figshare.com/s/6900f26033c71afc7888: Data analysed in this study. Appendix 1: Error distribution in the FM-100 diagram for post-COVID participants (N=77). Appendix 2: Computer program for calculating major and minor axes for the D-15, D-15d and FM 100-Hue tests. Supplementary Materials: Table S1 – Demographic characteristics of post-COVID participants, and self-reported duration of the illness and symptoms. Table S2 – FM-100 parameters for post-COVID participants: total error score (TES), error scores for four FM-100 boxes (AES, BES, CES, DES), and partial error scores (PES) for the specified hue bands, B-Y and R-G axes, and hemispheres of the FM-100 diagram: left (caps 1–43), right (caps 44–85), upper (caps 27–70) and lower (caps71–26). Figure S1 – FM-100 scores (ÖTES) for individual post-COVID participants as a function of age. For comparison, plotted are mean ÖTES scores for each age group of normal trichromats27,29,30, as presented in Table 1. Numbers accompanying points correspond to IDs of post-COVID participants, whose values exceed the lowest normal trichromats' mean. Table S3 – Spearman's correlation coefficient (p) between √PES in different hue bands and the number of days elapsed after the recovery of post-COVID participants. Figure S2 – √PES for post-COVID participants in different hemispheres of the FM-100 diagram: (a) √PES in left and right hemispheres; (b) √PES in upper and lower hemispheres; (c) √G–B – √R–Y difference (lower vs. upper hemisphere) as a function of the time elapsed after the participants' recovery. Zero difference is indicated by a solid horizontal line. Colour-coded are participants' age groups. Table S4 – The Vingrys and King-Smith indices of moment of inertia. Highlighted are values exceeding the cut-off values for normal trichromats, C-index >1.12 and S-index >1.38, and negative Angles, indicators of a tritan defect. Table S5 – Descriptive statistics of FM-100 indices for post-COVID participants (N=5) with negative Angle in comparison with mean values for 72 participants with positive Angle stratified as two groups in accord with the severity C-index cut-off value, C=1.12. Table S6 – Clusters of post-COVID participants based on their FM-100 performance, TES and the three parameters of moment of inertia35, obtained using the hierarchical clustering method. In each cluster, participants' IDs are given in colour, as coded in Figure 6. Highlighted (in grey) are individual participants' indices that assume an acquired (mild) colour vision deficiency: TES>90th percentile, C-index and S-index exceeding the cut-off values, negative and relatively low positive Angle.

Received: October 26, 2023
Revision received: December 10, 2023
Accepted: December 12, 2023

Author Contributions

Yulia Aleksandrovna Griber contributed to the study design; supervised the experiment, collected, analyzed and interpreted the data; participated in writing the manuscript and formatted it in line with the journal requirements.

Galina Vladimirovna Paramei contributed to the study design; wrote the Introduction, analyzed and interpreted the results; participated in writing the manuscript and in editing its English translation.

Author Details

Yulia Aleksandrovna Griber – Dr. Sci. (Cultural Studies), Professor, Department of Sociology and Philosophy, Director of the Color Lab Research and Education Center, Smolensk State University, Smolensk, Russian Federation; Scopus Author ID: 56809444600, ResearcherID: AAG-4410-2019, SPIN code: 8214-8269, ORCID: https://orcid.org/0000-0002-2603-5928; e-mail: y.griber@gmail.com

Galina Vladimirovna Paramei – Dr. habil. (Cognitive Psychology), Dr. habil. (Cognitive Neuroscience), Cand. Sci. (= PhD, General Psychology), Professor, Department of Psychology, Liverpool Hope University, Liverpool, United Kingdom; Scopus Author ID: 6602092654, ResearcherID: AAQ-7205-2020, ORCID: https://orcid.org/0000-0003-2611-253X; e-mail: parameg@hope.ac.uk

Conflict of Interest Information

The authors have no conflicts of interest to declare.